

Article

An EPR Study on Highly Stable Nitroxyl-Nitroxyl Biradicals for Dynamic Nuclear Polarization Applications at High Magnetic Fields

Nargiz B. Asanbaeva ¹, Sergey A. Dobrynin ¹ , Denis A. Morozov ¹, Nadia Haro-Mares ², Torsten Gutmann ² , Gerd Buntkowsky ²  and Elena G. Bagryanskaya ^{1,*} 

¹ N.N. Vorozhtsov Institute of Organic Chemistry, 9 Ac. Lavrentiev Avenue, Novosibirsk 630090, Russia

² TU Darmstadt, Eduard-Zintl-Institute for Inorganic and Physical Chemistry, Alarich-Weiss-Straße 8, 64287 Darmstadt, Germany

* Correspondence: egbagryanskaya@nioch.nsc.ru

Abstract: Nitroxide biradicals are efficient polarizing agents in dynamic nuclear polarization (DNP) solid-state nuclear magnetic resonance. Many recently reported radicals possess substantial DNP efficiency in organic solvents but have poor solubility in water media which is unfavorable for biological applications. In this paper, we report DNP efficiency at a high magnetic field for two water-soluble biradicals resistant to reducing media. Water solubility was achieved by obtaining the radicals in the form of quaternary ammonium salts. Parameters of *hyperfine interaction* and exchange interaction were quantified by EPR spectroscopy, and their influence on the DNP effect was determined. The resistance of the biradicals to strongly reducing media was characterized. High stability was achieved using tetraethyl substituents and pyrrolidine moieties.

Keywords: dynamic nuclear polarization; solid state NMR; EPR; biradicals



Citation: Asanbaeva, N.B.; Dobrynin, S.A.; Morozov, D.A.; Haro-Mares, N.; Gutmann, T.; Buntkowsky, G.; Bagryanskaya, E.G. An EPR Study on Highly Stable Nitroxyl-Nitroxyl Biradicals for Dynamic Nuclear Polarization Applications at High Magnetic Fields. *Molecules* **2023**, *28*, 1926. <https://doi.org/10.3390/molecules28041926>

Academic Editors:
Cristina Cantarutti,
Yamanappa Hunashal and
Gennaro Esposito

Received: 2 February 2023
Revised: 13 February 2023
Accepted: 15 February 2023
Published: 17 February 2023



Copyright: © 2023 by the authors. Licensee MDPI, Basel, Switzerland. This article is an open access article distributed under the terms and conditions of the Creative Commons Attribution (CC BY) license (<https://creativecommons.org/licenses/by/4.0/>).

1. Introduction

Solid-state NMR spectroscopy with magic-angle spinning (MAS) is a powerful method for obtaining essential structural information about biological samples. Nonetheless, the main problem with this method is its low sensitivity, due to the small nuclear spin population difference between ground and excited states in an applied magnetic field. Dynamic nuclear polarization (DNP) [1–4] is based on the polarization transfer, from highly polarized unpaired electron spins of polarizing agents (PAs) to nuclear spins (e.g., ¹H or ¹³C) of samples by microwave irradiation. This technique subsequently enhances the NMR signal-to-noise ratio; theoretically, up to 660-fold enhancement may be achieved for ¹H at a given temperature. PAs that are commonly used to gain the sensitivity of solid-state NMR experiments are biradicals. As mononitroxides or trityls, biradicals are employed to measure physiological parameters—pH [5] and oxygen, nitrogen oxide [6], and thiol concentrations [7]—in biological systems, but in recent decades they have found their main application in DNP NMR.

During the last decade, various groups of binitroxyls were synthesized and used as PAs: TOTAPOL [8–10], bcTol [10,11], AMUPols [12,13], SPIROPols [14,15], bTbk [16], TinyPols [17], AsymPols [18]; and as mixed biradicals: TEMTriPols [19], NATriPols [20], BDPA-based compounds [21–24], TN [25–27], and SNAPols [28]. Nonetheless, when working with such compounds, researchers encounter problems with their solubility in water and their resistivity to reductants, which is a crucial factor during biological sample preparation. Reduction of even one part of a biradical by a cell culture medium immediately leads to an inactive PA form and the failure of a cross-effect DNP experiment. For example, TOTAPOL, when utilized for studying native membranes, has shown a loss of DNP enhancement, likely because of reduction in the biradical by free cysteines [29]. Some

investigations of the resistance of most popular PAs to reduction have been carried out earlier [13,30]. It has been shown that increasing the intracellular stability of TOTAPOL or AMUPol is possible due to the addition of N-ethylmaleimide removing endogenous biothiols or regeneration of TOTAPOL by oxidation of its hydroxylamine forms. Although the nitroxides added to cells have been N-ethylmaleimide-protected, the stabilization of biradicals by this technique has not improved DNP performance. The stability of nitroxides correlated with the ring size and substituents neighboring the paramagnetic center [31]. In this paper, we study biradicals which have a skeleton based on five-membered-ring nitroxides and tetraethyl substituents that provide additional stability.

According to some reports, the highest DNP enhancement can be achieved due to the relatively strong exchange interaction (J) between the paramagnetic fragments in such biradicals [32]. Nonetheless, recent studies showed that the key factor for significant cross-effect DNP is not the great sum of exchange interaction and dipolar coupling (D), but the relative ratio J/D [33]. In addition, as shown earlier [34–36], DNP performance strongly depends on substituents around the radical center and on electron spin relaxation times. For biradicals with longer electron spin-relaxation times, higher DNP enhancement is observed. Thus, in many cases nitroxide biradicals with spirohexyl substituents possess high DNP enhancement. However, it was shown that when spirohexyl substituents do not provide accessibility of the solvent to the radical center, it leads to a decrease in DNP efficiency [36].

The aim of the present study is to continue the research into the development of effective polarization sources by determining structure–DNP performance relationships. Towards this goal, we investigated the application potential of biradicals **3** and **4** (Figure 1) in heteronuclear direct polarization experiments. In particular, the behavior of these biradicals in reducing media was analyzed, parameters of exchange interaction were measured, and the radicals were studied by DNP-enhanced solid-state NMR experiments to examine their efficiency at producing signal enhancement.

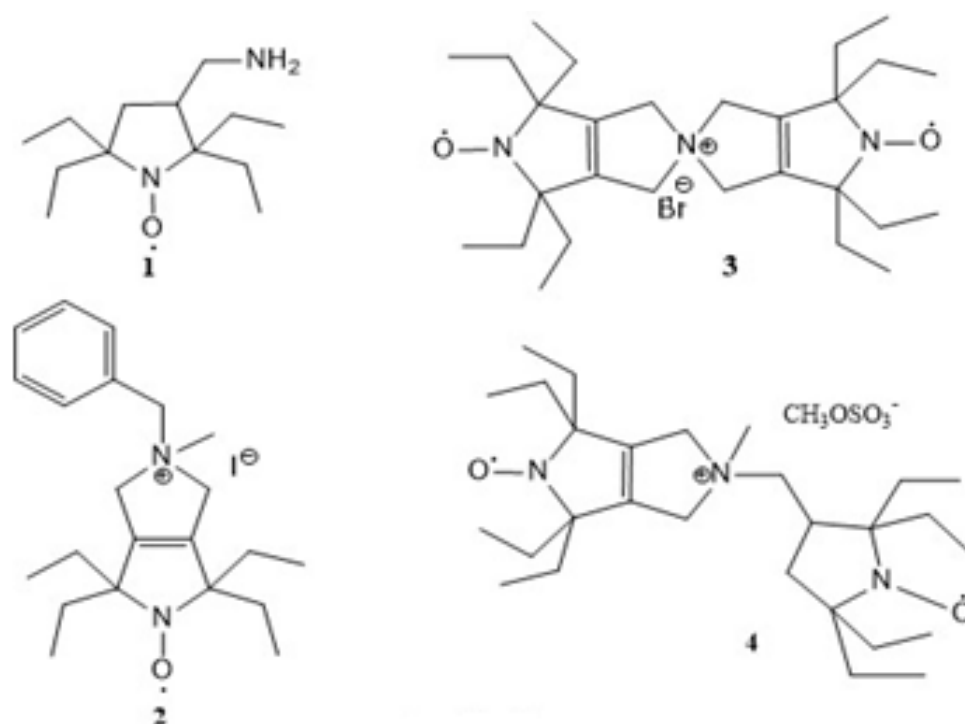


Figure 1. Chemical structures of monoradicals **1** and **2** and binitroxyl radicals **3** and **4**.

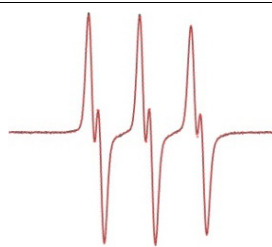
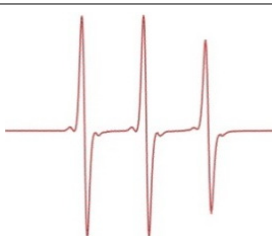
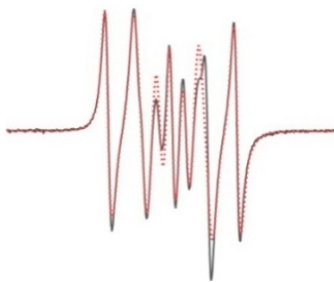
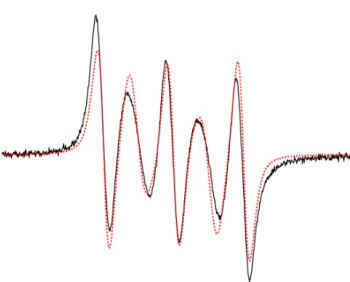
2. Results and Discussion

The synthetic procedures for radicals **2** and **4** have been previously described [37].

2.1. EPR Measurements and Simulations

To characterize the local structure of paramagnetic parts of the novel biradicals, we carried out room temperature (r.t.) X-band (9.87 GHz) continuous-wave EPR experiments on 100 μ M solutions in methanol or phosphate-buffered saline (PBS). All biradicals showed a multiplex splitting pattern in the solution, resulting in the superposition of hyperfine coupling to ^{14}N of the nitroxides ($A_{\text{N iso}}$) and the exchange interaction (J) between the two unpaired electrons. The observed X-band EPR spectra of all compounds are shown in Table 1 (column 2). Calculated EPR spectra were fitted to the exchange Hamiltonian expressed as $J \cdot S_1 \cdot S_2$. The obtained parameters (exchange coupling J and isotropic hyperfine A_{iso}) determined from the fitting analysis are listed in Table 1 (column 3).

Table 1. R.t. X-band EPR spectra of ~ 0.1 mM radicals 1–4.

Radical	EPR Spectrum	Parameters of Simulations
1	PBS 	$A_{\text{N iso}} = 43.0 \pm 0.2$ MHz $A_{\text{H iso}} = 7.2 \pm 0.2$ MHz
2	PBS 	$A_{\text{N iso}} = 43.7 \pm 0.2$ MHz
3	PBS 	$A_{\text{N iso}} = 43.7 \pm 0.2$ MHz $J = 206 \pm 2$ MHz
4	PBS 	$A_{\text{N1 iso}} = 44.0 \pm 0.2$ MHz $A_{\text{N2 iso}} = 43.2 \pm 0.2$ MHz $J = 0$ $\sigma(J) = 120$ MHz J distribution

Nitroxide-nitroxide biradicals. The EPR spectrum of the symmetric rigid biradical **3** can be fitted to $A_{N\text{ iso}} \approx 43.7$ MHz, $|J| = 206 \pm 2$ MHz (mean \pm SD), whereas for the asymmetric biradical **4**, simulations taking into account one value of exchange interaction failed. It should be noted that for similar biradicals, the authors of [36] have proposed two interpretations of the continuous-wave EPR spectrum. The first explanation is that the biradical is characterized only by zero mean exchange-coupling J , but a large width of the exchange-coupling distribution. This interpretation appears to be most probable, and the authors of [36] supported it by pulse EPR experiments. The second way to describe this data set requires an assumption of a considerable proportion of monoradicals present in the sample. We conducted a quantitative analysis of paramagnetic particles in the biradicals **3** and **4** relative to standard calibrated TEMPO and Finland trityl solutions by the CW EPR method. As a result of this experiment, it was determined that the concentration of paramagnetic spins in the solution corresponds to the assumption that all particles in the solution are in the form of biradicals. Therefore, we followed the first pathway of spectra interpretation, and good agreement between calculated and experimental EPR spectra was achieved by taking into account a J distribution with the center at $J = 0$ MHz and $\sigma(J) = 120$ MHz.

2.2. W-Band Echo-Detected Spectra

Pulsed EPR experiments at W-band (94 GHz) microwave (MW) frequency were acquired on a Bruker Elexsys E680X EPR spectrometer. In the experiments, $\pi/2$ pulse lengths of 16 ns were achieved. The experiments were carried out at a temperature of 80 K. ED spectra are shown on Figure 2.

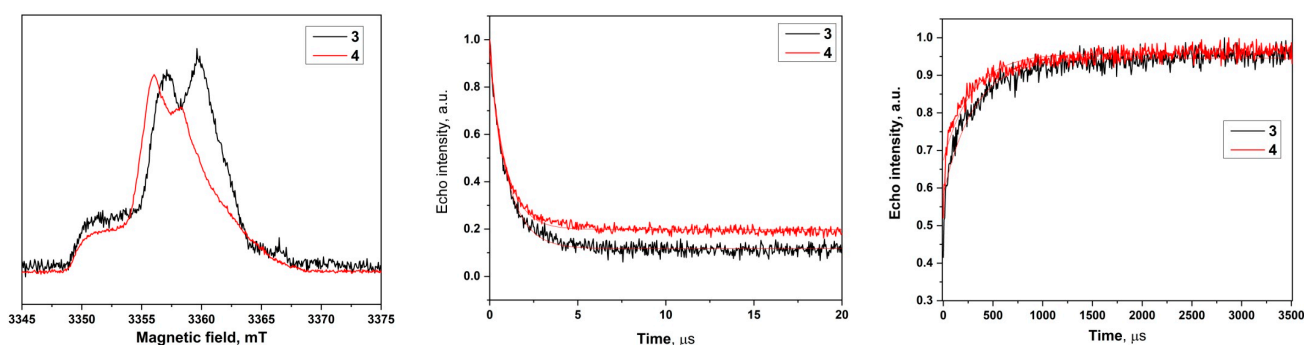


Figure 2. Left: The 94 GHz echo-detected EPR spectra (black: for **3**, red: for **4**) at 80 K. Center: Intensity of spin echo of biradicals **3–4** at 80 K as a function of the time. Right: Inversion recovery time traces of biradicals **3–4** at 80 K along with mono-exponential fits.

2.3. Relaxation Measurements

The spin–lattice relaxation time of the biradicals was measured by the inversion-recovery method (Supplementary Materials). The phase relaxation time of the samples was measured by means of primary echo decay. The obtained traces (Figure 2) were fitted by mono-exponential functions. The results of the fitting are presented in Table 2.

Table 2. Parameters of relaxation times for biradicals **3–4**.

Biradical	T_2 , μs	T_1 , ms
3	1.01 ± 0.01	0.31 ± 0.01
4	0.92 ± 0.01	0.29 ± 0.01

2.4. DNP Experiments

In Figure 3a,c, the ^1H MAS spectra obtained for radicals **3** and **4** in frozen glycerol- d_8 / $\text{D}_2\text{O}/\text{H}_2\text{O}$ (60:30:10 $v/v/v$) matrix are shown. The peak at 6.2 ppm is assigned to the isotropic signal from water present in the matrix. For radical **3**, an enhancement of

13 corresponding to a time saving factor of ca. 170 is obtained, which is slightly higher than the value of 9 observed for radical 4. In the $^1\text{H} \rightarrow ^{13}\text{C}$ CPMAS spectra (Figure 3b,d), signals at 60.7 and 70.5 ppm are observed, which are attributed to the aliphatic carbons of glycerol (also part of the matrix). An enhancement of 15 is achieved for radical 3 and an enhancement of 9 is obtained for radical 4. The similar enhancement factors obtained in the $^1\text{H} \rightarrow ^{13}\text{C}$ CPMAS and their corresponding ^1H MAS spectra clearly indicate a homogenous distribution of the two radicals in frozen solution.

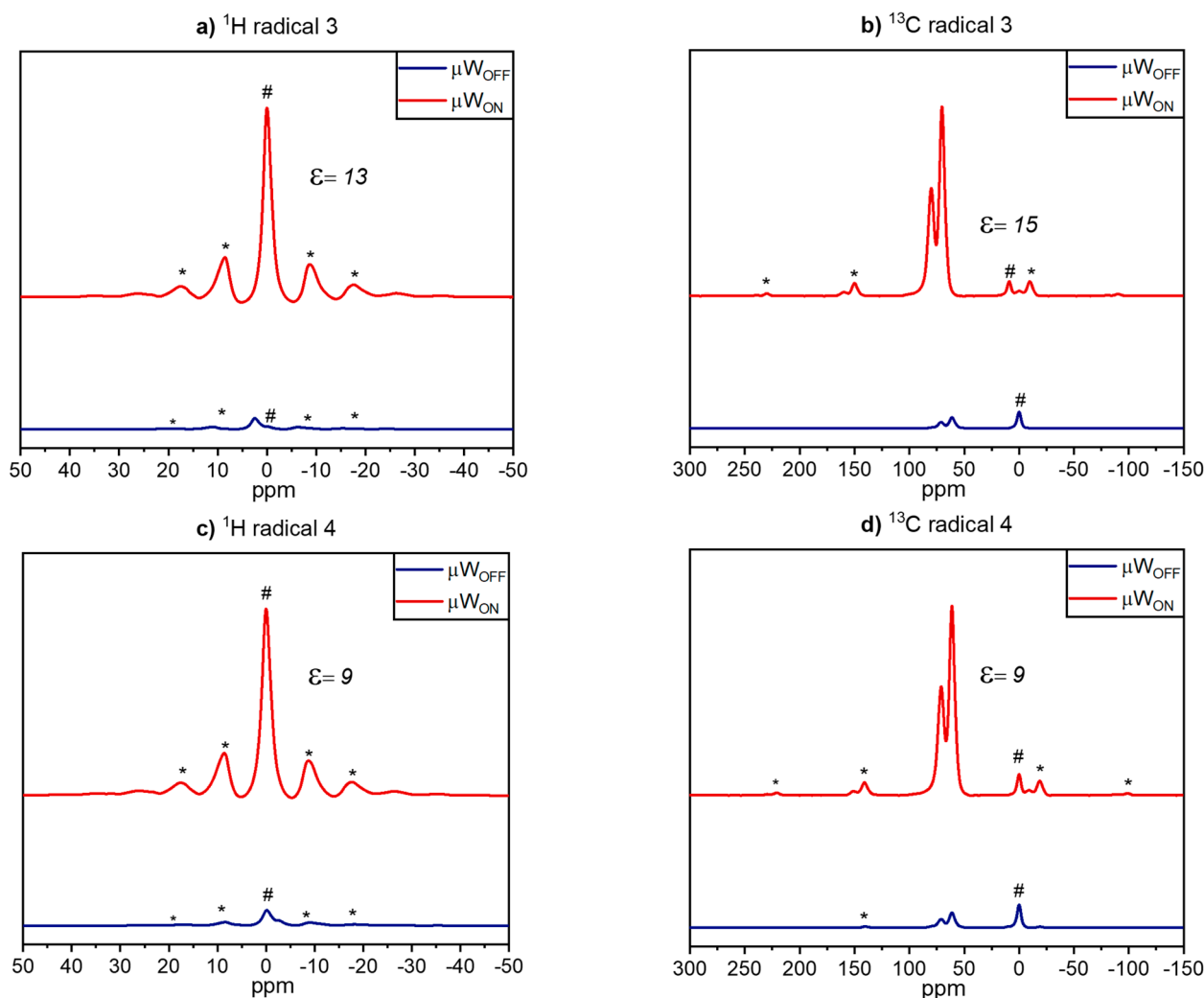


Figure 3. ^1H MAS and $^1\text{H} \rightarrow ^{13}\text{C}$ CPMAS spectra of frozen solutions of 15 mM binitroxyl radicals 3 (a,b) and 4 (c,d) in glycerol- $\text{d}_8/\text{D}_2\text{O}/\text{H}_2\text{O}$ (60:30:10 *v/v/v*). Spectra were recorded with (μW_{ON}) or without (μW_{OFF}) microwave irradiation at nominally 115 K. The # indicates the signal from the silicon plug near 0 ppm and the asterisks are attributed to spinning sidebands.

Build-up curves for radicals 3 and 4 in glycerol- $\text{d}_8/\text{D}_2\text{O}/\text{H}_2\text{O}$ (60:30:10 *v/v/v*) matrix are shown in Figure 4. Mono-exponential functions were used to fit the data points for both samples. For radical 3 (Figure 4a) a build-up time (T_{B}) of 1.10 ± 0.02 s and for radical 4 (Figure 4b) a T_{B} of 0.78 ± 0.03 s are calculated. The slightly shorter T_{B} obtained for radical 4 is in good agreement with the slightly smaller enhancement in the ^1H MAS spectrum obtained for radical 4 compared to radical 3.

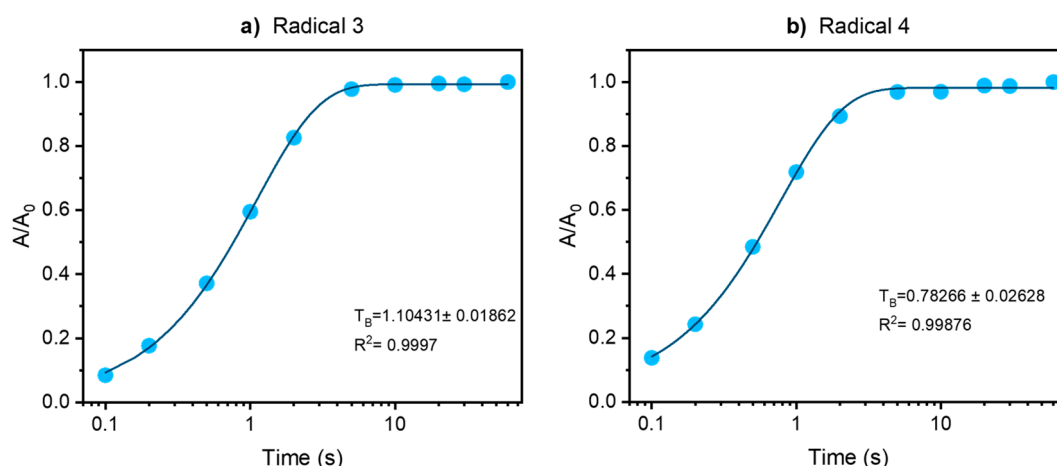


Figure 4. ^1H build-up curves obtained for frozen solutions of radical **3** (a) and **4** (b) in glycerol- d_8 / D_2O / H_2O (60:30:10 $v/v/v$). A mono-exponential function was used to fit the data points.

To investigate the polarization transfer in ^{13}C MAS NMR, spectra of biradicals **3** and **4** in glycerol- d_8 / D_2O / H_2O (60:30:10 $v/v/v$) matrix, measured with and without microwave irradiation with a build-up of 300 s, were recorded. To distinguish between direct and indirect polarization transfer, two sets of spectra were measured as described in the literature [38]. The results are shown in Figure 5. The indirect polarization pathway from electron to ^1H and then via cross-relaxation to ^{13}C in the μW_{OFF} spectra (Figure 5b,d) is almost negligible for radicals **3** and **4**. This observation is expected since the polarization transfer through cross-relaxation in solids is limited [39] and most of the time visible only via DNP enhancement. In the μW_{ON} spectra obtained for radical **3** (Figure 5a), the polarization transfer via the ^1H spin reservoir (indirect path) is clearly visible while for radical **4** (Figure 5c) there is no significant indirect path obtained. This indicates the presence of local motions in the frozen solution of radical **3**, while for radical **4** they are less pronounced. These differences are probably induced by the molecular structure of the radicals, an observation discussed in detail in our previous works [27,40].

Next to the indirect path for both radicals in frozen solutions the direct polarization transfer from electron to ^{13}C is observable. For these experimental data sets, an enhancement of 12 is obtained for radical **3** corresponding to a time saving factor of 144, while a value of 11 is reached for radical **4**.

If we compare the radicals, the amplification levels in the ^1H and the $^1\text{H} \rightarrow ^{13}\text{C}$ CPMAS spectra for radical **3** are larger than those for radical **4**. A probable reason is that biradical **3** almost completely consists of a structure with $J \approx 200$ MHz, in contrast to biradical **4**, which corresponds to the distribution of conformations centered at $J \approx 0$ MHz. As demonstrated earlier, the presence of conformers with $J \approx 0$ leads to a decrease in DNP efficiency [38]. In the ^{13}C MAS spectra, we observed comparable enhancements for radicals **3** and **4** for direct polarization transfer.

For both biradicals, the observed DNP enhancements are lower than for spiro substituted biradicals presented in [36]—an observation which is probably related to the electron spin relaxation time. To probe this assumption, we measured electron spin relaxation times at 9.7 T for biradicals **3** and **4**. We obtained similar values of ~ 1 μs (T_{2e}) and ~ 0.3 ms (T_{1e}) for biradicals **3** and **4** at a concentration of 0.1 mM at 80 K (Table 2). These values are at least two times shorter compared to spiro-substituted PAs [34–36]. Furthermore, we performed our DNP experiments with much higher biradical concentrations of 15 mM, where even shorter values of T_{2e} and T_{1e} are expected. These results are in good agreement with the authors' earlier work [41], where it was shown that spin relaxation times for radicals containing tetraethyl substituents are shorter compared to the corresponding radicals containing spiro substituents.

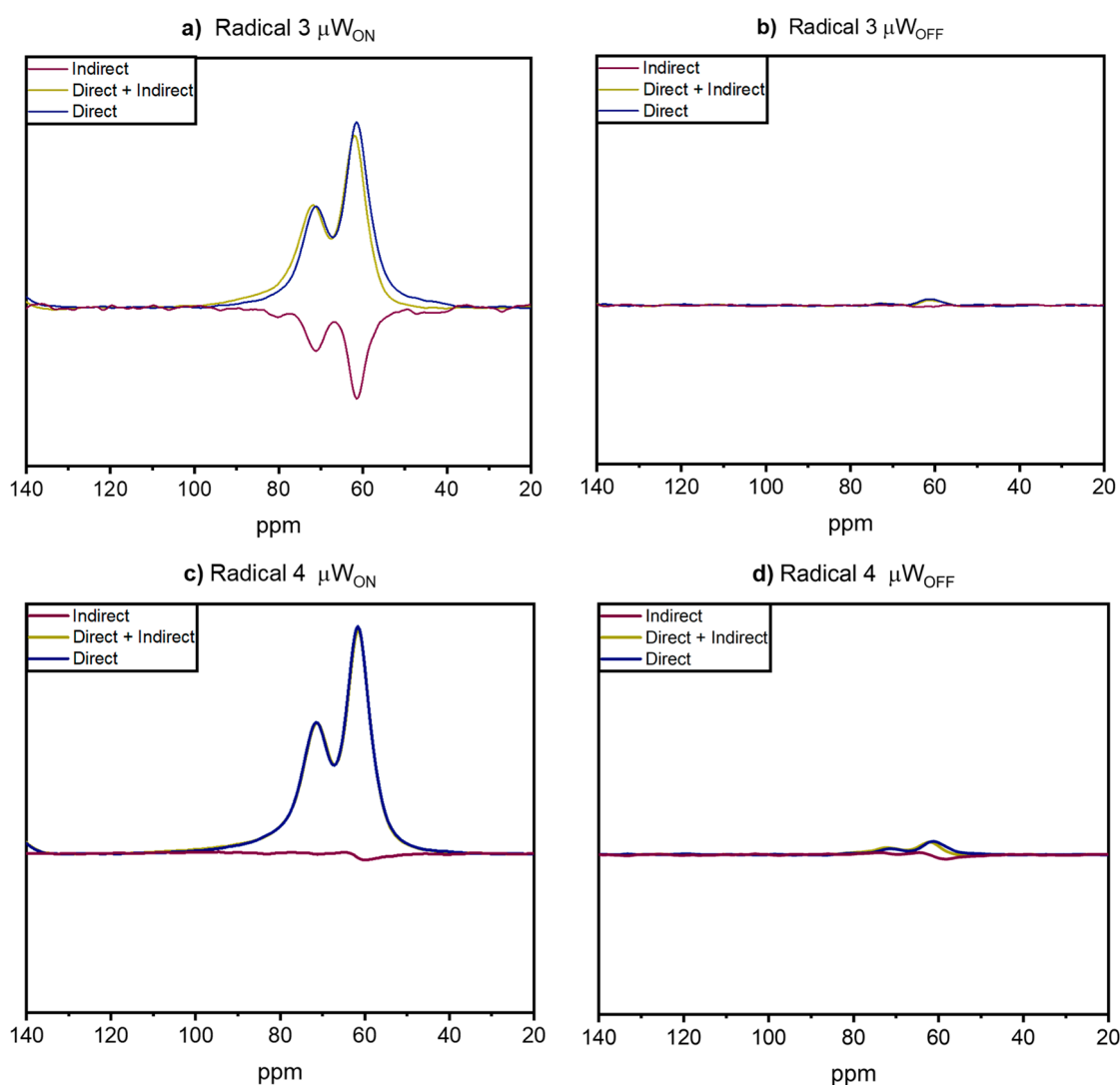


Figure 5. A ^{13}C MAS spectra of frozen solutions of 15 mM binitroxyl radicals **3** and **4**, respectively, in glycerol- $\text{d}_8/\text{D}_2\text{O}/\text{H}_2\text{O}$ (60:30:10 *v/v/v*) obtained with 300 s as build-up. (a) Radical **3** measured with MW irradiation (MW_{ON}), (b) radical **3** measured without MW irradiation (MW_{OFF}), (c) radical **4** with MW irradiation (MW_{ON}), and (d) radical **4** without MW irradiation (MW_{OFF}). Spectra were recorded at nominally 115 K.

Another probable important factor for the obtained DNP efficiency is the shielding of the radical center from solvents by tetraethyl substituents. Kubicki et al. [36] noted that for tetraethyl-containing biradicals, the optimum saturation factor ($T_{1e}T_{2e}$) can be reached, but the DNP enhancement is still low, which they explained by radical shielding. The structure of our tetraethyl nitroxides **3** and **4** obtained by X-ray [42,43] clearly shows that this “shielding” arises due to tetraethyl substituents, which form a dense shell at a distance of ~ 3 Å around the nitroxide moiety. On the other hand, it is this shielding that ensures tetraethyl nitroxide’s high stability against reduction by ascorbate or any other reducing agent, and allows their use in living systems and in the cells [44]. To underline this hypothesis, for our biradicals **3** and **4**, the resistance to reduction by ascorbic acid was inspected (for details see Section 2.3) showing that **3** and **4** are stable for several hours, in contrast to spiro-substituted PAs, which exist for only ~ 10 min in the presence of ascorbate [36].

2.5. Resistance of the Biradicals to Reduction by Ascorbate

To determine the rate of reduction of the biradicals, we added 0.1 M ascorbate at pH 7.4 to 0.3 mM radicals and measured the total signal intensity by EPR spectroscopy as a function of time. The integrated EPR signal reflects a total radical concentration, which, in the absence of reduction, is double the sample concentration. Because the two nitroxide moieties of **3** and **4** can be reduced independently, for precision, we reported this parameter as the total nitroxide concentration. The kinetics of radicals' **1–4** decay in the presence of 0.1 M ascorbate at pH 7.4 and are shown in Figure 6.

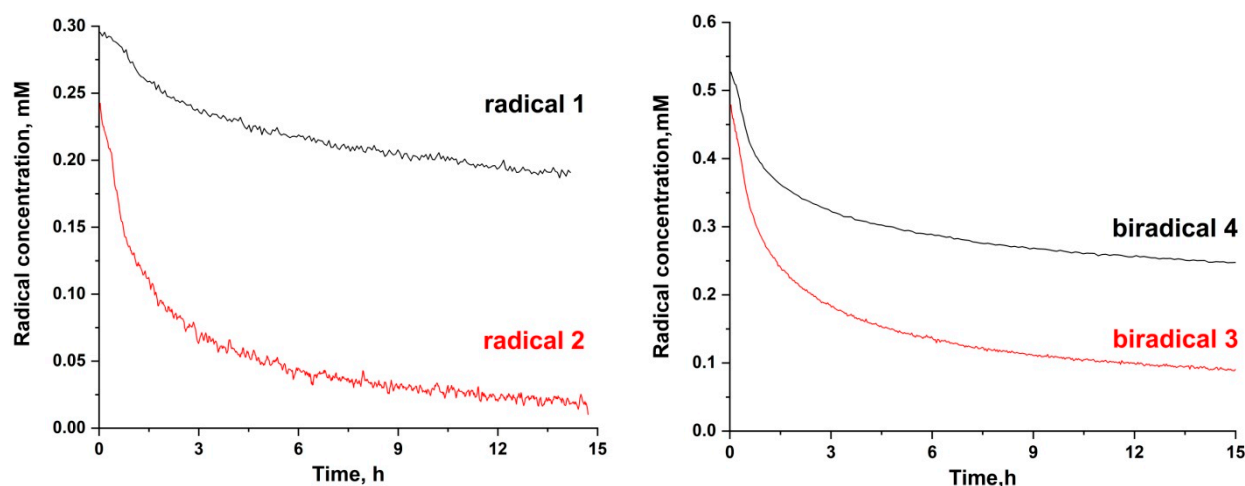


Figure 6. Kinetics of decay of radicals **1–4** in the presence of 0.1 M ascorbate in PBS at pH 7.4.

It is known that for highly stable nitroxides, the kinetics of reduction are complicated [45] and determined not only by the rate of nitroxide reduction but also by an equilibrium with hydroxylamine and the presence of a nascent ascorbate anion. Thus, to prevent the accumulation of the ascorbate anion, we chose the same approach as in the paper by Bobko et al. [43], and 2 mM glutathione was added into the solution. The initial part (60–120 min) of the kinetics of the decay was approximated to a mono-exponential function to calculate pseudo-first-order rate constants k_{obs} (Equation (1)):

$$I(t) = A_0 \cdot e^{-k_{obs} \cdot t} \quad (1)$$

After that, these constants k_{obs} were divided by the value of concentration of ascorbic acid to determine second-order reaction constants k . All reduction rate constants of the radicals are presented in Table 3. The rate constants were extracted from the initial part of the kinetics (60–120 min) when the contribution of indirect reactions was negligible [45].

Table 3. Rate constants of reduction by ascorbate for radicals **1–4** (for details, see the experimental part).

Radical	$k_{obs} \times 10^3, \text{min}^{-1}$	$k \times 10^3, \text{M}^{-1}\text{s}^{-1}$
1	1.4 ± 0.1	0.23 ± 0.02
2	11.6 ± 0.3	1.93 ± 0.05
3	9.7 ± 0.2	1.62 ± 0.03
4	6.2 ± 0.2	1.03 ± 0.03

As follows from the obtained data, the most stable radical is **1**. As one can see in Table 3, the reduction in biradicals **3** and **4** is limited by the reduction in the most stable paramagnetic moiety **2** and **1**, respectively.

In Figure 7, readers can observe a change of EPR spectra of biradical **4** in the presence of ascorbate. With time, the contribution of the monoradical part (three curves, black

arrows) increases and the exchange lines (two curves, red arrows) degrade. Moreover, magnetic-resonance parameters of the formed mononitroxide correspond to those of radical **1**. This observation is consistent with the finding that radical **2** is less stable than radical **1** (Table 3).

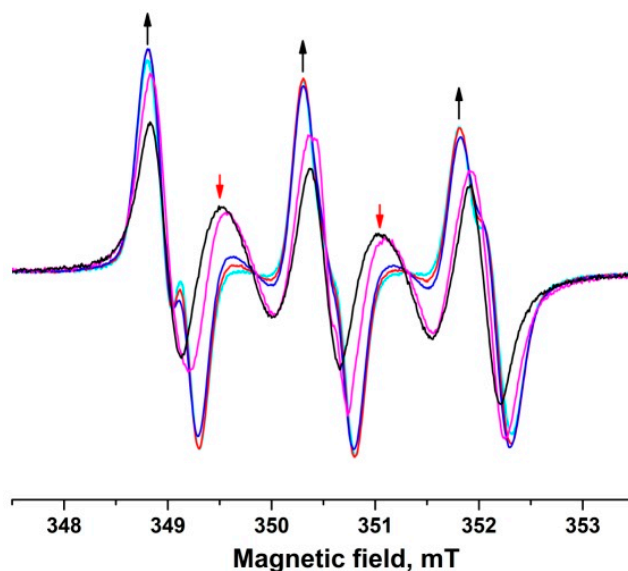


Figure 7. Kinetics of the decay of nitroxide biradical **4** in the presence of 0.1 M ascorbate in PBS at pH 7.4.

3. Materials and Methods

3.1. EPR Sample Preparation for W-Band EPR Experiments

EPR samples for W-band measurements of **3–4** were dissolved at a concentration of $\sim 100 \mu\text{M}$ in a mixture of deuterated DMSO and methanol (at 20:30, *v/v*) immediately before the experiments. Approximately $2 \mu\text{L}$ aliquots of these solutions were placed into quartz W-band EPR tubes (0.6 mm inner diameter, open at one end), which were shock-frozen in liquid nitrogen prior to insertion into the precooled cavity. The solvent mixtures used resulted in transparent, glassy samples upon rapid freezing.

3.2. X-Band EPR Experiments

CW electron paramagnetic resonance (EPR) spectra were recorded on a commercial Bruker (9 GHz) spectrometer, Elexsys E 540 (Bruker Corporation, Billerica, MA, USA), in water ($\sim 10^{-4}$ M for **1–4**) solutions in PBS, at pH 7.4, at room temperature. The EPR spectra were obtained with the following spectrometer settings: frequency, 9.87 GHz; microwave power, 0.5 mW; modulation amplitude, 0.05–0.15 mT for biradicals **1–4**; time constant, 20.5 ms; and conversion time, 20 ms. For kinetic measurements, the EPR spectra were performed at the same parameters but with a higher modulation amplitude (0.05–0.15 mT) to optimize the signal-to-noise ratio. Simulations of solution ESR lines were acquired in the EasySpin software 5.2.28 [46] (accessed on 16 May 2020), which is available at <http://www.easyspin.org>.

In order to measure reduction kinetics, stock solutions of a nitroxide radicals, ascorbic acid, and glutathione were prepared in phosphate buffer (10 mM, pH 7.4), and pH 7.4 was achieved with NaHCO_3 . All components were carefully and quickly mixed in a small tube to obtain required concentrations (radical: 0.3 mM, GSH: 2 mM, and ascorbate: 10–100 mM), and were inserted into an EPR capillary ($50 \mu\text{L}$). The capillary was closed on both sides and placed into the EPR resonator. The decay of integral intensity of the EPR spectrum was monitored to characterize the kinetics.

3.3. Solid-State DNP Experiments

3.3.1. Sample Preparation

For solid-state DNP experiments, 15 mM solutions of each binitroxyl radical (**3** and **4**) were prepared using a mixture of 60%v of glycerol- d_8 , 30%v of D_2O , and 10%v of H_2O as the matrix. Approximately 25 μL of each solution was packed into 3.2 mm sapphire rotors. To prevent any leakage, a silicon plug was placed between the liquid sample and the ZrO_2 drive cap.

3.3.2. DNP Experiments

All solid-state DNP experiments were performed on a Bruker Avance III 400 MHz NMR spectrometer equipped with an Ascend 400 sweep-able DNP magnet and a 3.2 mm triple resonance $^1H/X/Y$ low-temperature MAS probe. The microwave (μW) was provided by a 9.7 T Bruker gyrotron system operating at 263 GHz. Measurements were conducted at nominally 115 K in the presence (μW_{ON}) and absence (μW_{OFF}) of microwave irradiation. The 1H MAS, $^1H \rightarrow ^{13}C$ CPMAS, and ^{13}C MAS spectra were acquired at a spinning rate of 8 kHz.

To obtain 1H MAS spectra, a background suppression pulse sequence was used employing $\pi/2$ pulses with 2.3 μs and π pulses with 4.6 μs lengths [47]. A total of 16 scans were accumulated, and a relaxation delay of 4 s was applied.

The $^1H \rightarrow ^{13}C$ CPMAS experiments were performed with 128 scans, a recycle delay equal to $1.3 \cdot T_B$, where T_B is the build-up time for 1H , and a contact time of 2 ms. Spinal 64 heteronuclear proton decoupling was applied during data acquisition [48].

To obtain the build-up curves for 1H , the saturation–recovery pulse sequence was applied. This sequence starts with a saturation pulse train of twenty $\pi/2$ pulses with 2.3 μs length and 200 μs pulse spacing, followed by a waiting time to build up magnetization and a $\pi/2$ detection pulse. For each data point, 16 scans were accumulated. These measurements were performed with microwave irradiation (μW_{ON}).

The ^{13}C MAS direct polarization experiments were performed according to reference [49]. In all experiments, a saturation pulse train of fifteen $\pi/2$ pulses, each pulse with a length of 3.5 μs and a space of 5 ms between them was applied to the ^{13}C channel to have a defined initial magnetization. To select the direct polarization pathway, π pulses with a length of 6 μs with a spacing of 50 ms between them were applied to the proton channel to suppress polarization transfer via proton spin reservoir during the 300 s of build-up of the carbon magnetization. After that, a $\pi/2$ pulse of 3.5 μs was applied to the ^{13}C channel for detection. In contrast to the direct polarization pathway, the indirect polarization pathway cannot be detected separately. Thus, the indirect pathway was separated by subtracting the spectra obtained with π pulses on the 1H channel (showing only the direct path) from the spectrum obtained without π pulses on the 1H channel (showing the direct + indirect path). All experiments were carried out with (μW_{ON}) and without (μW_{OFF}) microwave irradiation for both radicals. A recycle delay of 0.5 s was used. During data acquisition, high-power proton decoupling was performed using the spinal 64 sequence [48].

To calculate the DNP enhancement factors (ϵ), the areas of the peaks obtained with μW_{ON} in the 1H MAS, the $^1H \rightarrow ^{13}C$ CPMAS and the ^{13}C MAS spectra, respectively, were divided by the corresponding peak areas obtained with μW_{OFF} .

4. Conclusions

An EPR study on two highly stable nitroxyl-nitroxyl biradicals was conducted, and their resistance to reduction by ascorbate in a buffer at pH 7.4 was characterized. The stability of the obtained DNP agents was very high due to tetraethyl substituents and pyrrolidine moieties. This, in principle, allows them to be used in cell biological experiments for several hours, which was not feasible with spiro-substituted biradicals. The observed DNP enhancement coefficients were substantial but not outstanding. One possible reason for these results are nonoptimal values of spin exchange interaction owing to flexible linkers. The second explanation is the fast electron spin relaxation induced by the tetraethyl

environment. Therefore, it is necessary to strike a balance between stability in biological media and a high DNP coefficient.

Supplementary Materials: The following are available online at <https://www.mdpi.com/article/10.3390/molecules28041926/s1>, Figure S1. 94 GHz echo-detected EPR spectra (black—for **3**, red—for **4**) at 80 K. Figure S2. Left: Intensity of spin echo of biradicals **3–4** at 80 K as a function of the time. Right: Inversion-recovery time traces of biradicals **3–4** at 80 K along with mono-exponential fits. Table S1. Parameters of relaxation times for biradicals **3–4**.

Author Contributions: Conceptualization, E.G.B. and G.B.; methodology, T.G.; investigation, N.B.A., S.A.D., N.H.-M. and D.A.M.; data curation, N.B.A., N.H.-M., S.A.D., D.A.M. and T.G.; writing—original draft preparation, N.B.A., T.G. and N.H.-M.; writing—review, editing and supervision, E.G.B. and G.B. All authors have read and agreed to the published version of the manuscript.

Funding: This research received no external funding.

Institutional Review Board Statement: Not applicable.

Informed Consent Statement: Not applicable.

Data Availability Statement: Not applicable.

Acknowledgments: The authors would like to acknowledge the Multi-Access Chemical Research Center SB RAS for spectral and analytical measurements. We thank the Ministry of Science and Higher Education of the Russian Federation for financial support. The authors are also grateful to Andrey Sukhanov (Zavoiky Physical–Technical Institute, Kazan, Russia) for the EPR measurements in the W band. G.B. and T.G. thank the Deutsche Forschungsgemeinschaft (DFG) under contract Bu-911-24/2 for their financial support.

Conflicts of Interest: The authors declare no conflict of interest.

References

1. Lilly Thankamony, A.S.; Wittmann, J.J.; Kaushik, M.; Corzilius, B. Dynamic Nuclear Polarization for Sensitivity Enhancement in Modern Solid-State NMR. *Prog. Nucl. Magn. Reson. Spectrosc.* **2017**, *102–103*, 120–195. [[CrossRef](#)] [[PubMed](#)]
2. Gutmann, T.; Groszewicz, P.B.; Buntkowsky, G. Solid-State NMR of Nanocrystals. *Annu. Rep. NMR Spectrosc.* **2019**, *97*, 1–82. [[CrossRef](#)]
3. Corzilius, B. High-Field Dynamic Nuclear Polarization. *Annu. Rev. Phys. Chem.* **2020**, *71*, 143–170. [[CrossRef](#)]
4. Perras, F.A.; Wang, L.L.; Manzano, J.S.; Chaudhary, U.; Opembe, N.N.; Johnson, D.D.; Slowing, I.I.; Pruski, M. Optimal Sample Formulations for DNP SENS: The Importance of Radical-Surface Interactions. *Curr. Opin. Colloid Interface Sci.* **2018**, *33*, 9–18. [[CrossRef](#)]
5. Ishiguro, K.; Ozaki, M.; Kamekura, Y.; Sekine, N.; Sawaki, Y. Preparation and Property of 2-(3',5'-Di-Tert-Butylphenyl-4'-Oxyl)-4,4,5,5-Tetramethyl-4,5, -Dihydro-1H-Imidazole-3-Oxide-1-Oxyl. *Mol. Cryst. Liq. Cryst.* **1997**, *306*, 75–80. [[CrossRef](#)]
6. Marx, L.; Rassat, A. Application of a Spin-Labeled Spin-Trap to the Detection of Nitric Oxide (NO). *Angew. Chem. Int. Ed.* **2000**, *39*, 4494–4496. [[CrossRef](#)]
7. Roshchupkina, G.I.; Bobko, A.A.; Bratasz, A.; Reznikov, V.A.; Kuppusamy, P.; Khramtsov, V.V. In Vivo EPR Measurement of Glutathione in Tumor-Bearing Mice Using Improved Disulfide Biradical Probe. *Free Radic. Biol. Med.* **2008**, *45*, 312–320. [[CrossRef](#)]
8. Song, C.; Hu, K.N.; Joo, C.G.; Swager, T.M.; Griffin, R.G. TOTAPOL: A Biradical Polarizing Agent for Dynamic Nuclear Polarization Experiments in Aqueous Media. *J. Am. Chem. Soc.* **2006**, *128*, 11385–11390. [[CrossRef](#)]
9. Nagaraj, M.; Franks, T.W.; Saeidpour, S.; Schubeis, T. Surface Binding of TOTAPOL Assists Structural Investigations of Amyloid Fibrils by Dynamic Nuclear Polarization NMR Spectroscopy. *ChemBioChem* **2016**, *17*, 1308–1311. [[CrossRef](#)]
10. Geiger, M.A.; Jagtap, A.P.; Kaushik, M.; Sun, H.; Stöppler, D.; Sigurdsson, S.T.; Corzilius, B.; Oschkinat, H. Efficiency of Water-Soluble Nitroxide Biradicals for Dynamic Nuclear Polarization in Rotating Solids at 9.4 T: BcTol-M and Cyolyl-TOTAPOL as New Polarizing Agents. *Chem. A Eur. J.* **2018**, *24*, 13485–13494. [[CrossRef](#)]
11. Jagtap, A.P.; Geiger, M.A.; Stöppler, D.; Orwick-Rydmark, M.; Oschkinat, H.; Sigurdsson, S.T. BcTol: A Highly Water-Soluble Biradical for Efficient Dynamic Nuclear Polarization of Biomolecules. *Chem. Commun.* **2016**, *52*, 7020–7023. [[CrossRef](#)]
12. Sauvée, C.; Casano, G.; Abel, S.; Rockenbauer, A.; Akhmetzhanov, D.; Karoui, H.; Siri, D.; Aussenac, F.; Maas, W.; Weber, R.T.; et al. Tailoring of Polarizing Agents in the BTurea Series for Cross-Effect Dynamic Nuclear Polarization in Aqueous Media. *Chem. A Eur. J.* **2016**, *22*, 5598–5606. [[CrossRef](#)] [[PubMed](#)]
13. Ghosh, R.; Dumariéh, R.; Xiao, Y.; Frederick, K.K. Stability of the Nitroxide Biradical AMUPol in Intact and Lysed Mammalian Cells. *J. Magn. Reson.* **2022**, *336*, 107150. [[CrossRef](#)] [[PubMed](#)]
14. Michaelis, V.K.; Keeler, E.G.; Bahri, S.; Ong, T.-C.; Daviso, E.; Colvin, M.T.; Griffin, R.G. Biradical Polarizing Agents at High Fields. *J. Phys. Chem. B* **2022**, *126*, 7847–7856. [[CrossRef](#)] [[PubMed](#)]

15. Kiesewetter, M.K.; Michaelis, V.K.; Walish, J.J.; Griffin, R.G.; Swager, T.M. High Field Dynamic Nuclear Polarization NMR with Surfactant Sheltered Biradicals. *J. Phys. Chem. B* **2014**, *118*, 1825–1830. [[CrossRef](#)] [[PubMed](#)]
16. Zagdoun, A.; Casano, G.; Ouari, O.; Schwarzwälder, M.; Rossini, A.J.; Aussenac, F.; Yulikov, M.; Jeschke, G.; Copéret, C.; Lesage, A.; et al. Large Molecular Weight Nitroxide Biradicals Providing Efficient Dynamic Nuclear Polarization at Temperatures up to 200 K. *J. Am. Chem. Soc.* **2013**, *135*, 12790–12797. [[CrossRef](#)] [[PubMed](#)]
17. Lund, A.; Casano, G.; Menzildjian, G.; Kaushik, M.; Stevanato, G.; Yulikov, M.; Jabbour, R.; Wissner, D.; Renom-Carrasco, M.; Thieuleux, C.; et al. TinyPols: A Family of Water-Soluble Binitroxides Tailored for Dynamic Nuclear Polarization Enhanced NMR Spectroscopy at 18.8 and 21.1 T. *Chem. Sci.* **2020**, *11*, 2810–2818. [[CrossRef](#)]
18. Harrabi, R.; Halbritter, T.; Aussenac, F.; Dakhlaoui, O.; van Tol, J.; Damodaran, K.K.; Lee, D.; Paul, S.; Hediger, S.; Mentink-Vigier, F.; et al. Highly Efficient Polarizing Agents for MAS-DNP of Proton-Dense Molecular Solids. *Angew. Chem. Int. Ed.* **2022**, *61*, e202114103. [[CrossRef](#)]
19. Mathies, G.; Caporini, M.A.; Michaelis, V.K.; Liu, Y.; Hu, K.N.; Mance, D.; Zweier, J.L.; Rosay, M.; Baldus, M.; Griffin, R.G. Efficient Dynamic Nuclear Polarization at 800 MHz/527 GHz with Trityl-Nitroxide Biradicals. *Angew. Chem. Int. Ed.* **2015**, *54*, 11770–11774. [[CrossRef](#)]
20. Zhai, W.; Lucini Paioni, A.; Cai, X.; Narasimhan, S.; Medeiros-Silva, J.; Zhang, W.; Rockenbauer, A.; Weingarth, M.; Song, Y.; Baldus, M.; et al. Postmodification via Thiol-Click Chemistry Yields Hydrophilic Trityl-Nitroxide Biradicals for Biomolecular High-Field Dynamic Nuclear Polarization. *J. Phys. Chem. B* **2020**, *124*, 9047–9060. [[CrossRef](#)]
21. Wissner, D.; Karthikeyan, G.; Lund, A.; Casano, G.; Karoui, H.; Yulikov, M.; Menzildjian, G.; Pinon, A.C.; Porea, A.; Engelke, F.; et al. BDPA-Nitroxide Biradicals Tailored for Efficient Dynamic Nuclear Polarization Enhanced Solid-State NMR at Magnetic Fields up to 21.1 T. *J. Am. Chem. Soc.* **2018**, *140*, 13340–13349. [[CrossRef](#)]
22. Dane, E.L.; Maly, T.; Debelouchina, G.T.; Griffin, R.G.; Swager, T.M. Synthesis of a BDPA-TEMPO Biradical. *Org. Lett.* **2009**, *11*, 1871–1874. [[CrossRef](#)]
23. Mandal, S.; Sigurdsson, S.T. On the Limited Stability of BDPA Radicals. *Chem. A Eur. J.* **2020**, *26*, 7486–7491. [[CrossRef](#)]
24. Mandal, S.; Sigurdsson, S.T. Water-Soluble BDPA Radicals with Improved Persistence. *Chem. Commun.* **2020**, *56*, 13121–13124. [[CrossRef](#)]
25. Liu, Y.; Villamena, F.A.; Rockenbauer, A.; Zweier, J.L. Trityl-Nitroxide Biradicals as Unique Molecular Probes for the Simultaneous Measurement of Redox Status and Oxygenation. *Chem. Commun.* **2010**, *46*, 628–630. [[CrossRef](#)]
26. Liu, Y.; Villamena, F.A.; Song, Y.; Sun, J.; Rockenbauer, A.; Zweier, J.L. Synthesis of ¹⁴N- and ¹⁵N-Labeled Trityl-Nitroxide Biradicals with Strong Spin-Spin Interaction and Improved Sensitivity to Redox Status and Oxygen. *J. Org. Chem.* **2010**, *75*, 7796–7802. [[CrossRef](#)]
27. Bothe, S.; Nowag, J.; Klimavičius, V.; Hoffmann, M.; Troitskaya, T.I.; Amosov, E.V.; Tormyshev, V.M.; Kirilyuk, I.; Taratayko, A.; Kuzhelev, A.; et al. Novel Biradicals for Direct Excitation Highfield Dynamic Nuclear Polarization. *J. Phys. Chem. C* **2018**, *122*, 11422–11432. [[CrossRef](#)]
28. Cai, X.; Lucini Paioni, A.; Adler, A.; Yao, R.; Zhang, W.; Beriashvili, D.; Safeer, A.; Gurinov, A.; Rockenbauer, A.; Song, Y.; et al. Highly Efficient Trityl-Nitroxide Biradicals for Biomolecular High-Field Dynamic Nuclear Polarization. *Chem. A Eur. J.* **2021**, *27*, 12758–12762. [[CrossRef](#)]
29. Linden, A.H.; Lange, S.; Franks, W.T.; Akbey, Ü.; Specker, E.; van Rossum, B.-J.; Oschkinat, H. Neurotoxin II Bound to Acetylcholine Receptors in Native Membranes Studied by Dynamic Nuclear Polarization NMR. *J. Am. Chem. Soc.* **2011**, *133*, 19266–19269. [[CrossRef](#)]
30. McCoy, K.M.; Rogawski, R.; Stovicek, O.; Mcdermott, A.E. Stability of Nitroxide Biradical TOTAPOL in Biological Samples. *J. Magn. Reson.* **2019**, *303*, 115–120. [[CrossRef](#)]
31. Kirilyuk, I.A.; Bobko, A.A.; Semenov, S.V.; Komarov, D.A.; Irtegov, I.G.; Grigorev, I.A.; Bagryanskaya, E. Effect of Sterical Shielding on the Redox Properties of Imidazoline and Imidazolidine Nitroxides. *J. Org. Chem.* **2015**, *80*, 9118–9125. [[CrossRef](#)]
32. Mentink-Vigier, F.; Marin-Montesinos, I.; Jagtap, A.P.; Halbritter, T.; Van Tol, J.; Hediger, S.; Lee, D.; Sigurdsson, S.T.; De Paëpe, G. Computationally Assisted Design of Polarizing Agents for Dynamic Nuclear Polarization Enhanced NMR: The AsymPol Family. *J. Am. Chem. Soc.* **2018**, *140*, 11013–11019. [[CrossRef](#)]
33. Equbal, A.; Tagami, K.; Han, S. Balancing Dipolar and Exchange Coupling in Biradicals to Maximize Cross Effect Dynamic Nuclear Polarization. *Phys. Chem. Chem. Phys.* **2020**, *22*, 13569–13579. [[CrossRef](#)]
34. Kubicki, D.J.; Casano, G.; Schwarzwälder, M.; Abel, S.; Sauvée, C.; Ganesan, K.; Yulikov, M.; Rossini, A.J.; Jeschke, G.; Copéret, C.; et al. Rational Design of Dinitroxide Biradicals for Efficient Cross-Effect Dynamic Nuclear Polarization. *Chem. Sci.* **2016**, *7*, 550–558. [[CrossRef](#)]
35. Zagdoun, A.; Casano, G.; Ouari, O.; Lapadula, G.; Rossini, A.J.; Lelli, M.; Baffert, M.; Gajan, D.; Veyre, L.; Maas, W.E.; et al. A Slowly Relaxing Rigid Biradical for Efficient Dynamic Nuclear Polarization Surface-Enhanced NMR Spectroscopy: Expedient Characterization of Functional Group Manipulation in Hybrid Materials. *J. Am. Chem. Soc.* **2012**, *134*, 2284–2291. [[CrossRef](#)]
36. Stevanato, G.; Casano, G.; Kubicki, D.; Rao, Y.; Esteban Hofer, L.; Menzildjian, G.; Karoui, H.; Siri, D.; Cordova, M.; Yulikov, M.; et al. Open and Closed Radicals: Local Geometry Around Unpaired Electrons Governs MAS DNP Performance. *J. Am. Chem. Soc.* **2020**, *142*, 16587–16599. [[CrossRef](#)]

37. Fehling, P.; Buckenmaier, K.; Dobrynin, S.A.; Morozov, D.A.; Polienko, Y.F.; Khoroshunova, Y.V.; Borozdina, Y.; Mayer, P.; Engelmann, J.; Scheffler, K.; et al. The Effects of Nitroxide Structure upon 1H Overhauser Dynamic Nuclear Polarization Efficacy at Ultralow-Field. *J. Chem. Phys.* **2021**, *155*, 144203. [[CrossRef](#)]
38. Asanbaeva, N.B.; Gurskaya, L.Y.; Polienko, Y.F.; Rybalova, T.V.; Kazantsev, M.S.; Dmitriev, A.A.; Gritsan, N.P.; Haro-Mares, N.; Gutmann, T.; Buntkowsky, G.; et al. Effects of Spiro-Cyclohexane Substitution of Nitroxyl Biradicals on Dynamic Nuclear Polarization. *Molecules* **2022**, *27*, 3252. [[CrossRef](#)]
39. White, J.L.; Haw, J.F. Nuclear Overhauser Effect in Solids. *J. Am. Chem. Soc.* **1990**, *112*, 5896–5898. [[CrossRef](#)]
40. Hoffmann, M.M.; Bothe, S.; Gutmann, T.; Buntkowsky, G. Unusual Local Molecular Motions in the Solid State Detected by Dynamic Nuclear Polarization Enhanced NMR Spectroscopy. *J. Phys. Chem. C* **2017**, *121*, 22948–22957. [[CrossRef](#)]
41. Kuzhelev, A.A.; Strizhakov, R.K.; Krunkacheva, O.A.; Polienko, Y.F.; Morozov, D.A.; Yu, G.; Pyshnyi, D.V.; Kirilyuk, I.A.; Fedin, M.V.; Bagryanskaya, E.G. Room-Temperature Electron Spin Relaxation of Nitroxides Immobilized in Trehalose: Effect of Substituents Adjacent to NO-Group. *J. Magn. Reson.* **2016**, *266*, 1–7. [[CrossRef](#)] [[PubMed](#)]
42. Dobrynin, S.A.; Glazachev, Y.I.; Gatilov, Y.V.; Chernyak, E.I.; Salnikov, G.E.; Kirilyuk, I.A. Synthesis of 3,4-Bis(Hydroxymethyl)-2,2,5,5-Tetraethylpyrrolidin-1-Oxyl via 1,3-Dipolar Cycloaddition of Azomethine Ylide to Activated Alkene. *J. Org. Chem.* **2018**, *83*, 5392–5397. [[CrossRef](#)] [[PubMed](#)]
43. Paletta, J.T.; Pink, M.; Foley, B.; Rajca, S.; Rajca, A. Synthesis and Reduction Kinetics of Sterically Shielded Pyrrolidine Nitroxides. *Org. Lett.* **2012**, *14*, 5322–5325. [[CrossRef](#)]
44. Ovcherenko, S.S.; Chinak, O.A.; Chechushkov, A.V.; Dobrynin, S.A.; Kirilyuk, I.A.; Krunkacheva, O.A.; Richter, V.A.; Bagryanskaya, E.G. Uptake of Cell-Penetrating Peptide RL2 by Human Lung Cancer Cells: Monitoring by Electron Paramagnetic Resonance and Confocal Laser Scanning Microscopy. *Molecules* **2021**, *26*, 5442. [[CrossRef](#)] [[PubMed](#)]
45. Bobko, A.A.; Kirilyuk, I.A.; Grigor'ev, I.A.; Zweier, J.L.; Khramtsov, V.V. Reversible Reduction of Nitroxides to Hydroxylamines: Roles for Ascorbate and Glutathione. *Free Radic. Biol. Med.* **2007**, *42*, 404–412. [[CrossRef](#)] [[PubMed](#)]
46. Stoll, S.; Schweiger, A. EasySpin, a Comprehensive Software Package for Spectral Simulation and Analysis in EPR. *J. Magn. Reson.* **2006**, *178*, 42–55. [[CrossRef](#)] [[PubMed](#)]
47. Cory, D.G.; Ritchey, W.M. Suppression of Signals from the Probe in Bloch Decay Spectra. *J. Magn. Reson.* **1988**, *80*, 128–132. [[CrossRef](#)]
48. Comellas, G.; Lopez, J.J.; Nieuwkoop, A.J.; Lemkau, L.R.; Rienstra, C.M. Straightforward, Effective Calibration of SPINAL-64 Decoupling Results in the Enhancement of Sensitivity and Resolution of Biomolecular Solid-State NMR. *J. Magn. Reson.* **2011**, *209*, 131–135. [[CrossRef](#)]
49. Hoffmann, M.M.; Bothe, S.; Brodrecht, M.; Klimavicius, V.; Haro-Mares, N.B.; Gutmann, T.; Buntkowsky, G. Direct and Indirect Dynamic Nuclear Polarization Transfer Observed in Mesoporous Materials Impregnated with Nonionic Surfactant Solutions of Polar Polarizing Agents. *J. Phys. Chem. C.* **2020**, *124*, 5145–5156. [[CrossRef](#)]

Disclaimer/Publisher's Note: The statements, opinions and data contained in all publications are solely those of the individual author(s) and contributor(s) and not of MDPI and/or the editor(s). MDPI and/or the editor(s) disclaim responsibility for any injury to people or property resulting from any ideas, methods, instructions or products referred to in the content.